# LES OF 3-D TURBULENT WAVY BOUNDARY FLOW: VALIDATION OF A GHOST-CELL IMMERSED BOUNDARY METHOD

**Yu-Heng Tseng, Joel H. Ferziger**
Environmental Fluid Mechanics Laboratory,
Stanford University
Stanford, CA 94305-4020, USA
yhtseng@stanford.edu, ferziger@ecoule.stanford.edu

## ABSTRACT

Large-eddy simulation (LES) is used to investigate three-dimensional turbulent flow over a wavy boundary. An efficient immersed boundary method (IBM) for simulating turbulent flows in complex geometries is presented. The method is based on a finite-volume approach on a non-staggered Cartesian mesh and a fractional-step method. A force is applied on the body surface through an immersed ghost cell method. The reconstruction procedure allows systematic development of numerical schemes that preserve the overall second-order accuracy of the base solver. The accuracy of the current method is validated by comparing with previous boundary-fitted grid results (Zedler and Street, 2001). Both steady and unsteady flows are simulated. A steady flow simulation provides not only the mean and turbulence statistics but also visualization of the Görtler vortices. The unsteady oscillatory flow displays the three-dimensional vortex formation/transport cycle which is shown to be important for sediment transport.

## INTRODUCTION

In computational fluid dynamics, the primary issues are accuracy, computational efficiency, and the handling of complex geometry. Most large scale geophysical flows involve complex three-dimensional geometry and turbulence. Accurate representation of multi-scale, time dependent physical phenomena is a principal concern. The development of accurate and efficient methods that can deal with complex geometry would represent a significant advance. The immersed boundary method (IBM) has recently been demonstrated to be applicable to complex geometries, requiring significantly less computation than competing methods without sacrificing accuracy and stability (Fadlun et al., 2000). The method specifies a body force in such a way as to simulate the presence of a surface without altering the computational grid. The main advantages of the IBM are memory and CPU savings and ease of grid generation compared to unstructured grid methods. Bodies of arbitrary shape can be treated.

In this study, we extend the idea of Fadlun et al. (2000) via a ghost cell approach. It promises to provide the flexibility needed for imposing various boundary conditions. The approach imposes the specified boundary condition by interpolating the variable to a ghost node inside the body. In order to verify the accuracy of the IBM, two-dimensional flow over a circular cylinder has been treated. In this paper, we apply this approach to LES of three-dimensional turbulent flow over a wavy boundary and compare with boundary-fitted grid results (Zedler and Street, 2001). The purpose of this study is to illustrate the flexibility of the IBM and to assess the numerical procedures. The computational requirements (both CPU and memory) are significantly lower than a boundary-fitted grid. Furthermore, some important features of the flow over the wavy boundary are identified and explained.

## NUMERICAL SIMULATION

### Numerical formulation

Large eddy simulation is employed to simulate the turbulent wavy boundary flow. The N-S equations are solved using a finite-volume technique. The method of fractional steps (a variant of the projection method), which splits the numerical operators and enforces continuity (Kim and Moin, 1985) by solving a pressure Poisson equation, is used. All spatial derivatives are discretized using central differences with the exception of convective term. That term is discretized using QUICK (Leonard, 1979) in which the velocity components on the cell faces are computed from the nodal values using a quadratic interpolation scheme. Details of the method can be found in Zang (1993) and Tseng and Ferziger (2001). For three-dimensional turbulent flows at high Reynolds number, it is not possible to resolve all of the spatial and temporal scales. We solve for the large scale motions while fluctuations at scales smaller than the filter width are modeled using a subfilter-scale model. The subgrid scale (SGS) term $\tau_{ij}$ is modeled with Zang's dynamic mixed model (Zang et al., 1993). The scale-similarity term allows backscatter and the Smagorinsky component provides dissipation.

### Ghost cell method for immersed boundary

Mohd-Yusof (1997) suggested an approach that introduces a body-force field $f$ such that the desired velocity distribution $V$ is obtained at the boundary $\Omega$. In principle, there are no restrictions on the velocity distribution $V$ or the motion of $\Omega$. He implemented the method for a complex geometry in a pseudo-spectral code while avoiding the need of a small computational time step. The method costs no more than the base computational scheme. Fadlun et al. (2000) applied this approach to a three-dimensional finite-difference method on a staggered grid and showed that the approach was more efficient than feedback forcing. They also successfully implemented the immersed boundary algorithm in LES of turbulent flow in a motored axisymmetric piston-cylinder assembly (Verzicco et al., 2000). This approach does not reduce the stability of the underlying time-integration scheme and very good quantitative agreement with experimental measurements was obtained. For comparable accuracy, the computational requirements are

reduced by at least a factor of ten compared to simulations on an unstructured, boundary-fitted mesh (Verzicco et al., 2000).

In this paper, we develop an alternative approach through use of a ghost zone. In order to represent the complex boundary on a Cartesian grid, a boundary forcing term $f_i$ is added to the momentum equation implicitly through ghost cells (Tseng and Ferziger, 2003). The present approach is more flexible with respect to the incorporation of boundary conditions. The immersed boundary and a ghost cell zone are illustrated in Fig. 1(a). We express the flow variables in terms of a polynomial and use it to evaluate the ghost point values. We use linear and quadratic approaches which preserve the second-order accuracy of the overall numerical scheme. The scheme is equally applicable to steady and moving boundaries. In the case of moving bodies, the points at which the boundary condition is enforced must be recomputed at every time step but this does not affect the reconstruction scheme.

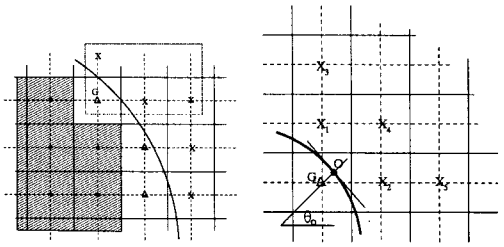

(a) (b)

Figure 1: (a) Schematic of computational domain with an immersed boundary. x: point in the physical domain, $\Delta$: the ghost cell domain. (b) Schematic of the points used to evaluate the variable located at a ghost cell point $G$.

**Linear reconstruction.**

The simplest approach in 2-D is to construct a triangle with the ghost node and the two nearest fluid nodes as the vertices. This choice minimizes the probability of numerical instability. In Fig. 1(b), $G$ is the ghost node, $X_1$ and $X_2$ are the two nearest fluid nodes and $O$ is the node at which the boundary condition is to be satisfied. $O$ can be chosen as the midpoint of the boundary segment within the cell or the point on the boundary at which $\overrightarrow{GO}$ is normal to the boundary. A linear interpolation in 2D is:

$$\phi = a_0 + a_1 x + a_2 y \tag{1}$$

The ghost cell value is a weighted combination of the values at the nodes ($X_1$, $X_2$ and $O$). The coefficients can be expressed in terms of the nodal values:

$$a^t = B^{-1}\phi^t \tag{2}$$

where, for linear interpolation, $B$ is a $3 \times 3$ matrix whose elements can be computed from the coordinates of the three points. When the velocity at the boundary is specified:

$$B = \begin{bmatrix} 1 & x_0 & y_0 \\ 1 & x_1 & y_1 \\ 1 & x_2 & y_2 \end{bmatrix}.$$

It is convenient to evaluate the matrices $B$ at each point initially and store them for use during the solution procedure. The major drawback with this extrapolation is that large negative weighting coefficients are encountered when the boundary point is close to one of the fluid nodes used in the extrapolation. Although algebraically correct, this can lead to numerical instability. This problem can be overcome by using the image of the ghost node inside the flow domain to ensure positive weighting coefficients. The oint $I$ is the image of the ghost node $G$ through the boundary as shown in Fig. 2. The flow variable is evaluated at the image point using the interpolation scheme. The value at the ghost node is then $\phi_G = 2\phi_O - \phi_I$. This ensures that large negative weighting coefficients will not occur.

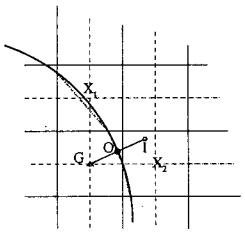

Figure 2: Schematic of a ghost cell using the image method (**I** is the image point) to minimize numerical instability.

**Quadratic reconstruction.**

Most second-order accurate finite volume flow solvers assume quadratic variation of flow variables near the wall. Use of higher order interpolation retains the formal second order accuracy of the scheme. In two dimensions, if the flow variables are assumed to vary in a quadratic manner in both the $x$ and $y$ directions, the value of $\phi$ is expressed as

$$\phi = a_0 + a_1 x + a_2 y + a_3 x^2 + a_4 xy + a_5 y^2 \tag{3}$$

The six constants of the assumed polynomial are evaluated from five neighboring fluid nodes and the wall point (Fig. 1(b)). The matrix $B$ in (2) is replaced by a $6 \times 6$ matrix. The reconstruction procedure is similar to that for the linear polynomial. The influence of the schemes on the overall accuracy is compared in Fig. 3 for uniform flow past a two-dimensional cylinder (Tseng and Ferziger, 2003). The results suggest that the accuracy is second-order for both the linear and quadratic interpolation, i.e. the order is not affected by the boundary treatment. For three dimensional boundaries, we need to modify the interpolation schemes (1) and (3). More neighbor nodes are involved but the remainder of the solution procedure remains the same as that described above.

It is important to note that for the forcing of Goldstein et al. (1993), the velocity at the immersed boundaries was imposed by canceling a few terms in the equations. This implies that, in contrast to the feedback forcing method, the stability limit of the integration scheme is the same as that without the immersed boundaries, thus making simulation of complex three-dimensional flows practical.

The method computes the velocity value just inside the boundary using the neighboring points. With the polynomial reconstruction scheme, we do not solve any equations on the ghost cells. In the non-staggered Cartesian grid approach, the treatment for Dirichlet boundary conditions has been described. A similar scheme can be used for Neumann boundary conditions. The only difference is in the construction of matrix $B$ in (2). This makes the current approach applicable to a variety of boundary conditions and the approach can be easily extended to larger scale flows.

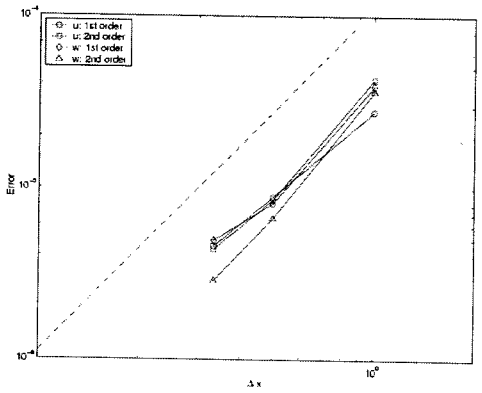


Figure 3: $L_\infty$ norm error of the streamwise ($u$) and spanwise ($v$) velocity components vs. the computational grid size. $\circ$, $\diamond$: linear polynomial reconstruction, $\square$, $\Delta$: quadratic polynomial reconstruction.

For example, the pressure boundary condition requires the wall normal derivative to be zero at the boundary:

$$\frac{\partial P}{\partial n}|_\Omega = 0 \tag{4}$$

The normal derivative on the boundary can be decomposed as

$$\frac{\partial P}{\partial n} = \frac{\partial P}{\partial x}\hat{n}_x + \frac{\partial P}{\partial y}\hat{n}_y \tag{5}$$

where $\hat{n}_x$ and $\hat{n}_y$ are the components of the unit vector normal to the boundary. Since $\hat{n}_x$ and $\hat{n}_y$ are known, the computation of the normal gradient is trivial. The same strategy can be extended to staggered Cartesian grid (Tseng and Ferziger, 2003).

It is worth pointing out here how our methodology differs from the immersed boundary method of Ye et al. (1999) and Fadlun et al. (2000). First, the interpolation scheme differs from theirs. Second, the reshaped cell method in Ye et al. (1999) complicates the numerical algorithm and the extension to other boundary conditions and moving boundaries is difficult. Third, the current approach uses ghost cells rather than reshaped cells to enforce the boundary condition.

Note that this method does not require any internal treatment of the body except the ghost cells since a fractional step is used and the forcing is only on the boundary. Internal treatment was required by Goldstein et al. (1993) and Mohd-Yusof (1997) in their spectral simulations to alleviate the problem of spurious oscillations near the boundary.

### Convergence of the Poisson solver

The flow solver uses a pressure correction method to satisfy the continuity equation. For high Reynolds numbers and highly stretched grids, it is difficult to converge the Poisson equation to machine accuracy. When we simulate complex geometry using IBM, the slow convergence is further exacerbated because the immersed boundary modifies the linear system. Krylov subspace methods are an attractive alternative approach. The presence of the immersed boundary poses no additional complication for these methods. The convergence rate of these procedures depends critically on the choice of the preconditioner. The convergence of point Gauss-Seidel, Bi-CGSTAB, Bi-CGSTAB with an ILU preconditioner and Bi-CGSTAB with the SIP preconditioner is shown in Fig. 4. The incomplete factorization preconditioning (both ILU and SIP) for Bi-CGSTAB accelerates the convergence significantly. The SIP preconditioner shows a dramatic reduction in iteration number and is used in all calculations shown below.

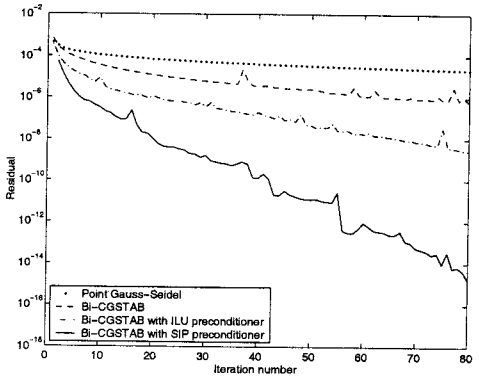


Figure 4: The convergence rate of point Gauss-Seidel, Bi-CGSTAB, Bi-CGSTAB with ILU preconditioner and Bi-CGSTAB with SIP preconditioner applied to the pressure equation for the simulation of 3-D turbulent flow over wavy boundary.

## NUMERICAL RESULTS

### Description of the simulations

The results using IBM described in previous section are compared with the results of Zedler and Street (2001) who used a non-orthogonal, boundary-fitted grid to compute turbulent flow over a wavy boundary. Their results have been compared with laboratory experiments for the same geometry (Calhoun and Street, 2001). The bottom boundary configuration mimics straight crested transverse ripples of form $A\sin(2\pi x/\lambda)$, where $A = 0.254$ $cm$ is the ripple amplitude and $\lambda = 5.08$ $cm$ is the ripple wavelength. The domains are roughly the same with dimensions of 20.3 $cm \times 4.8$ $cm \times 2.1$ $cm$ ($L \times W \times H$) as shown in Fig. 5. Two cases are used to illustrate the application of IBM. The steady flow is driven by a uniform pressure gradient that yields Reynolds number of about 2500, based on the channel height of 2.1 $cm$ and the mean streamwise velocity. The unsteady flow is driven by an oscillatory pressure gradient that yields the same Reynolds number based on the maximum velocity. The boundary conditions are periodic on all lateral boundaries, free-slip (zero stress) at the top and no-slip at the wavy bottom.

### Steady flow simulations

For purposes of comparing with boundary-fitted grid results, vertical profiles at five location in one wavelength of the topography are shown. The mean streamwise velocities and Reynolds shear stress are compared in Figs. 6(a) and (b) respectively. The differences between the IBM and boundary-fitted profiles for the mean streamwise velocities are very small. In particular, the profiles in the outer regions (beyond $(y - y_0) = 0.3h$, $y_0$ being the height of bottom topography) identified by Calhoun and Street (2001) are almost identical. A detailed comparison of the mean streamwise velocities in the vicinity of the crest is shown in Fig. 7. The differences between the average velocity profiles over the crest are small. The Reynolds stress ($-\overline{u'v'}$) at each location in the simulation using IBM compares well with the boundary-fitted grid profile (Fig. 6(b)).

The contours of mean vertical velocity from the IBM

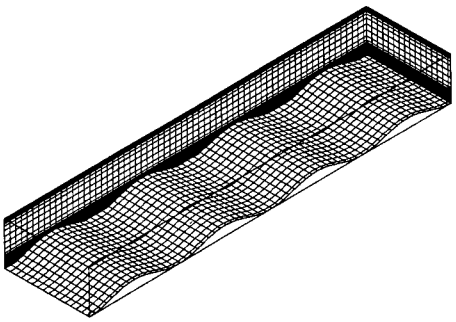

Figure 5: The computational domain for the wavy channel flow; the domain size is 20.3 $cm \times 2.1\ cm \times 4.8\ cm$. The bottom wavy boundary is derived from the boundary-fitted grid (every second grid point in each direction is shown).

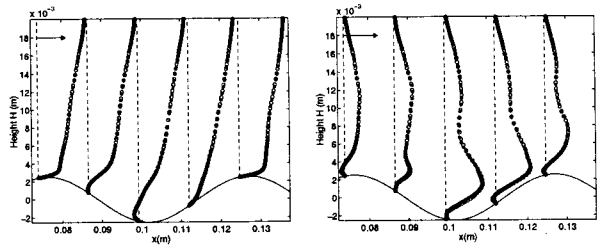

(a) (b)

Figure 6: (a) Comparisons of streamwise velocity profile from the IBM and boundary-fitted grid results for steady flow. The arrow at the top denotes 0.1 $m/s$ ($0.56U_{max}$). (b) Comparisons of turbulent Reynolds stress between the IBM and boundary-fitted grid results for steady flow. The arrow at the top denotes 0.0002 $m^2/s^2$. o: boundary-fitted grid results and $*$: IBM results.

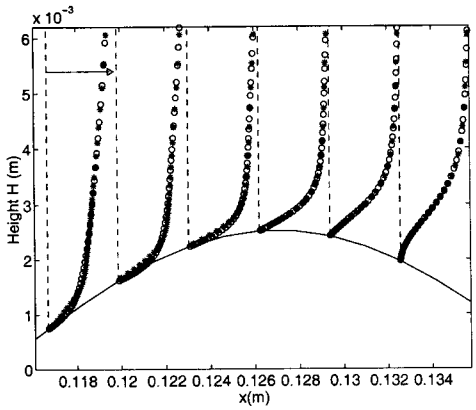


Figure 7: Comparisons of streamwise velocity profile between the IBM and boundary-fitted grid results for steady flow in the vicinity of the crest. o: boundary-fitted grid results and $*$: IBM results.

and boundary-fitted grid results are compared in Fig. 8. The agreement is very good. Positive velocity is denoted by the solid contours and negative velocity by the dashed ones. The vertical velocity is more sensitive to the method than the streamwise velocity since its magnitude is much smaller. The recirculation is apparent in the mean vertical velocity contour as positive vertical velocities on the downward sloping portion of the surface. The vertical velocity contours obtained with the IBM are very similar to the contours produced by boundary-fitted grid.

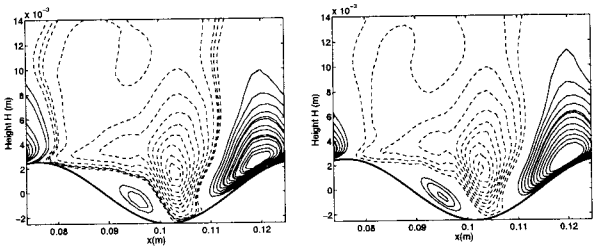

(a) (b)

Figure 8: Comparisons of mean vertical velocity contours between the IBM and boundary-fitted grid results for steady flow over one wavelength of the topography. (a) IBM (b) boundary-fitted grid. $--$: negative velocity, $-$: positive velocity.

In order to illustrate the structure of the instantaneous vortex cores we have plotted contours of the second invariant of the velocity gradient tensor (Jeong and Hussain, 1995) in Fig. 9. This approach is a variation of pressure minimum method. The vortex cores resemble those in channel flow, but they are longer, taller and have a greater angle of inclination (Calhoun and Street, 2001). These vortices result from the Görtler instability associated with boundary curvature. A detailed description of these vortices can be found in previous studies (Calhoun and Street, 2001; Zedler and Street, 2001). The current study identifies the same structures, indicating that this method adequately resolves turbulent boundary layer.

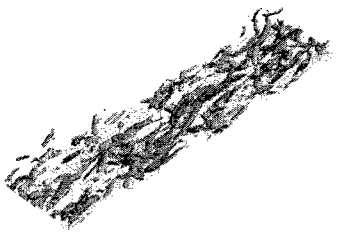

Figure 9: Instantaneous snapshot of vortex cores plotted as isocontours of $\lambda_2 = -50$ in fully developed steady wavy flow with the IBM approach.

Contours of the components of the turbulence intensity (TI) are shown in Fig. 10. The maximum streamwise $\overline{u'^2}$ is found above the center of the trough and is associated with the shear layer that detaches from the surface at the separation point. Contours of vertical TI show that the maximum is located slightly downstream of the location of the maximum of the streamwise TI. The maximum value is about

one third of the streamwise value. Henn and Sykes (1999) noted an increase in spanwise velocity fluctuations on the upstream slopes of their wavy boundary and suggested that the precise mechanism responsible is not yet known. Calhoun and Street (2001) concluded that Görtler instability appears to be important in the formation of the vortices and associated with the increase in spanwise velocity fluctuation. As shown in Fig. 10(b), the spanwise TI shows a marked increase on the upslope close to the wavy surface. The magnitude and location suggests a localized production mechanism associated with the waviness of the boundary. These features confirm the link between the streamwise vortices and the increase of spanwise TI found by Calhoun and Street (2001).

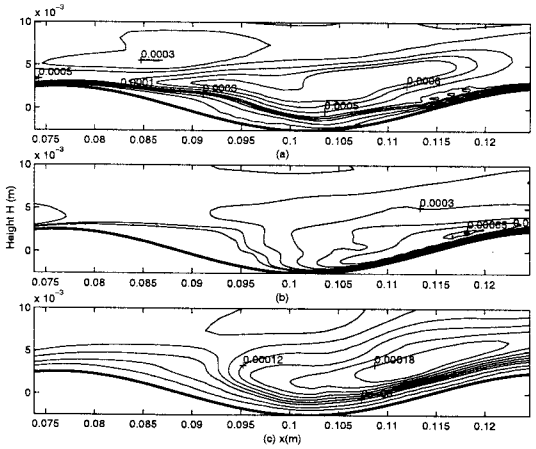


Figure 10: Contours of mean flow turbulence intensity. (a) Streamwise turbulence intensity $\overline{u'^2}$ (b) Spanwise turbulence intensity $\overline{v'^2}$ (c) Vertical turbulence intensity $\overline{w'^2}$.

### Unsteady flow simulations

We also simulated the unsteady flow over a wavy boundary produced by an oscillatory pressure gradient. A small recirculation zone forms just before the pressure gradient has attained its maximum negative value. As the flow slows down due to the adverse pressure gradient, spanwise vortices form and are lifted off the bottom to roughly the height of the wave crests. Quantitative comparisons between the IBM approach and boundary-fitted grid results of the spanwise-averaged streamwise velocity at four time steps are given in Fig. 11. These velocity profiles are phase averaged over ten cycles to obtain stable statistics. Sample taking starts after the flow reaches an oscillatory steady state. The mean profiles show good agreement with boundary-fitted simulations.

Fig. 12 provides the instantaneous, spanwise-averaged velocity vector field at $t = 0.25T$. The time $t = 0$ corresponds to the maximum pressure gradient. Recirculation zones appear behind the ripple crests in the instantaneous velocity vector plot but are confined to the bottom few grid points. These are similar to vortices obtained with boundary-fitted grids (Zedler and Street, 2001). The flow behavior in both the steady and unsteady cases in the current study is nearly the same as that in studies that used boundary-fitted grids (Calhoun and Street, 2001; Zedler and Street, 2001), indicating that the present method accurately captures the three-dimensional turbulent flow field.

Fig 13 presents the vortex formation/transport process by showing the vortex cores at different time steps. The formation cycle occurs twice per period, on either side of a

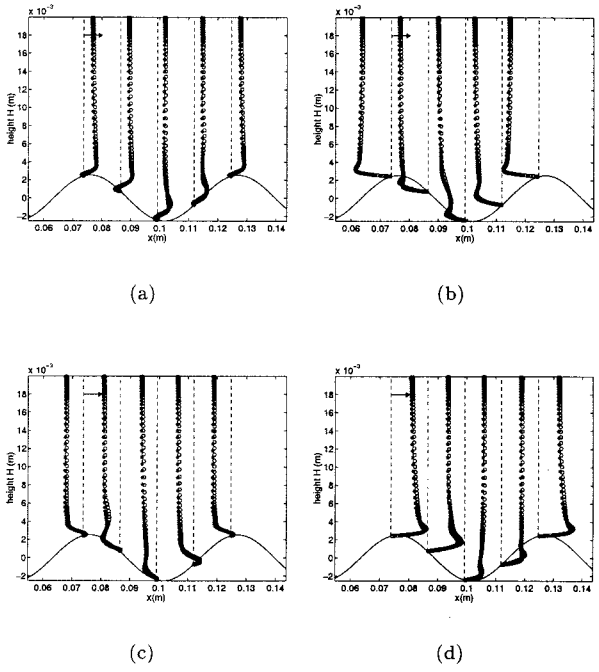


Figure 11: Comparison of streamwise velocity at different time steps. (a) t=0.25T (b) t=0.5T (c) t=0.75T (d) t=T. T is the time period imposed by the oscillatory pressure gradient. ∘ denotes the boundary-fitted grid result and ∗ denotes the IBM result.

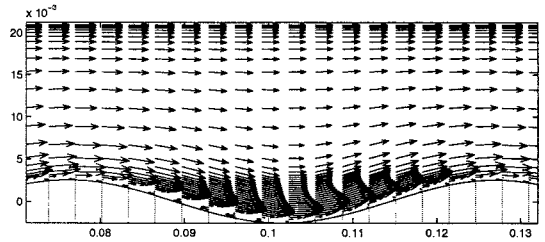

Figure 12: Instantaneous, spanwise-averaged velocity vector plot at $t = 0.25T$ using IBM. (every second grid point in each direction is shown).

wave trough. It starts as the flow accelerates ($t/T = 0.25$) and forms the recirculation zone. The vortex structures are generated by boundary layer separation and the growth of three-dimensional disturbances (Scandura et al., 2000). These structures are advected downstream as the flow slows down. As the flow slows down, the boundary layer on the lee side thickens and the recirculation zone is lifted away from the bottom. Some of the vortices are centered over the trough. This structure breaks up into a more complex, three-dimensional structure as the flow slows further. After the flow switches direction ($t/T = 0.5$), these complex structures are lifted off the bottom and advected over the crest (Fig. 13(c)). They are stretched in the streamwise direction and lose some of their strength as the flow accelerates in the other direction ($t/T = 0.75$). Then the process repeats in the other direction. The current results are very similar to those simulated in Scandura et al. (2000) and the nonlinear effects appear important for the growth of three dimensional instability.

## CONCLUSIONS

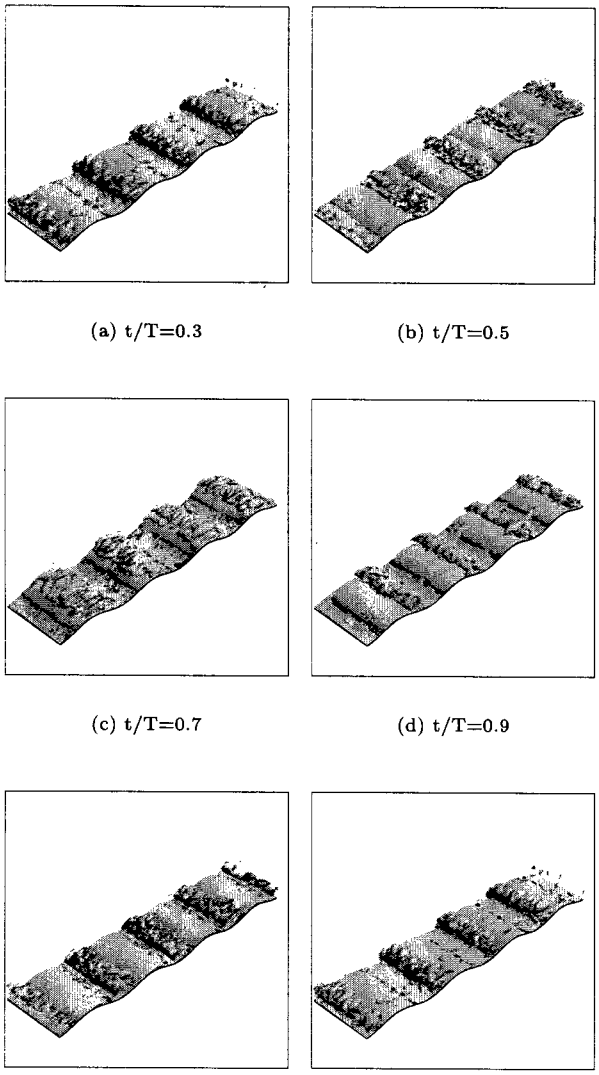

(a) t/T=0.3 (b) t/T=0.5

(c) t/T=0.7 (d) t/T=0.9

(e) t/T=1.1 (f) t/T=1.3

Figure 13: Vortex structures plotted with the $\lambda_2$ method for different flow phases during a time period $T(t/T = 0.3$ to $t/T = 1.3)$. $t/T = 0, 1$ corresponds to the phase of maximum oscillatory pressure gradient. The vortices are localized between two contiguous wave crests.

The aim of this study was to develop and apply an ghost cell immersed boundary method for LES of turbulence over a wavy boundary. Both steady and unsteady flows were simulated and compared with established numerical simulations done on a boundary-fitted grid. The entire computation including the body forces are done on a structured orthogonal mesh. The forcing was imposed by introducing ghost-cells inside the boundary and does not reduce the stability limit of the time-advance scheme. These simulation results agree well with previous numerical and experimental results, indicating the validity and accuracy of the present method. Many structures in flows over a wavy boundary were identified and investigated in the current study.

## ACKNOWLEDGEMENTS

The authors would like to thank Dr. Robert L. Street and Dr. Emily Zedler for their invaluable help and continuous support with the turbulent flow simulation. Finacial support for this work was provided by NSF ITR/AP (GEO) grant number 0113111 (Ms. B. Fossum, Program Manager) and NASA AMES/Center for Turbulent Research, Stanford.

## REFERENCES

Calhoun, R. J., and Street, R. L., 2001, "Turbulent flow over a wavy surface: Neutral case," *J. Geophys. Res.*, Vol. 106, pp. 9277-9293.

Fadlun, E. A., Verzicco, R., Orlandi, P., and Mohd-Yusof, J., 2000, "Combined immersed-boundary finite-difference methods for three-dimensional complex flow simulations," *Journal of Comput. Phys.*, Vol. 161, pp. 30-60.

Goldstein, D. Handler, R., and Sirovich, L., 1993, "Modeling a no-slip flow boundary with an external force field," *Journal of Comput. Phys.*, Vol. 105, pp. 354-366.

Henn, D., and Sykes, I., 1999, "Large-eddy simulation of flow over wavy surfaces," *J. Fluid Mech.*, Vol. 383, pp. 75-112.

Kim, J., and Moin, P., 1985, "Application of a fractional-step method to incompressible Navier-Stokes equations", *Journal of Comput. Phys.*, Vol. 59, pp.308-323.

Leonard, B. P., 1979, "A stable and accurate convective modeling procedure based on quadratic upstream interpolation Third-order multi-dimensional Euler/Navier-Stokes solver", *Comp. Methods Appl. Mech. Engr.*, Vol. 19, pp. 58-98.

Mohd-Yusof, J,, 1997, "Combined immersed boundary/B-Spline Methods for simulations of flows in complex geometries", CTR Annual Research Briefs, NASA Ames Research Center/Stanford Univ, Center for Turbulent Research, Stanford, CA.

Scandura, P., Vittori, G., and Blondeaux, P., 2000, "Three-dimensional oscillatory flow over steep ripples," *J. Fluid Mech.*, Vol. 412, pp. 355-378.

Tseng, Y. H., and Ferziger, J. H., 2001 "Effects of coastal geometry and the formation of cyclonic/anti-cyclonic eddies on turbulent mixing in upwelling simulation," *J. Turbulence*, Vol. 2, 14.

Tseng, Y. H., and Ferziger, J. H., 2003 "A ghost-cell immersed boundary method for flow in complex geometry", *Submitted to J. Comput. Phys.*

Verzicco, R., Mohd-Yusof, J., Orlandi, P., and Haworth, D., 2000, "Large eddy simulation in complex geometry configurations using boundary body forces", *AIAA Journal*, Vol. 38, pp. 427-433.

Ye, T., Mittal, R., Udaykumar, H. S., and Shyy, W., 1999, "An accurate Cartesian grid method for viscous incompressible flows with boundary body forces", *Journal of Comput. Phys.*, Vol. 156, pp. 209-240.

Zang, Y., 1993, *On the development of tools for the simulation of geophysical flows*, PhD thesis, Stanford University.

Zang, Y., Street, R. L., and Koseff, J. R., 1993, "A dynamic mixed subgrid-scale model and its application to turbulent recirculating flows," *Phys. Fluids*, Vol. A(5), pp. 3186-3196

Zang, Y., and Street, R. L., 1995, "Numerical simulation of coastal upwelling and interfacial instability of a rotating and stratified fluid", *J. Fluid Mech.*, Vol. 305, pp. 47-75.

Zedler, E., and Street, R. L., 2001, "Large-eddy simulation of sediment transport: Currents over ripples," *J. Hydrau. Eng.*, Vol. 127, pp. 444-452.